Research Square

Preprints are preliminary reports that have not undergone peer review.
They should not be considered conclusive, used to inform clinical practice,
or referenced by the media as validated information.

ReaxFF molecular modeling of hemp lignin transformations in supercritical CO_2–ethanol–water compared with 2D HSQC NMR observations

Yunhao Zhang
South China University of Technology
Yanhong Feng
yhfeng@scut.edu.cn
South China University of Technology
Bo Lei
Hubei Engineering University
He Zhang
South China University of Technology
Guizhen Zhang
South China University of Technology
Xiaochun Yin
South China University of Technology
Bo Wu
National Industrial Innovation Center of Polymer Materials Co., Ltd

Research Article

Keywords: lignin, reactive molecular dynamics, ReaxFF, supercritical carbon dioxide, solvent effects, HSQC NMR

Posted Date: November 26th, 2026

DOI: https://doi.org/10.21203/rs.3.rs-11779485/v1

License: This work is licensed under a Creative Commons Attribution 4.0 International License.
Read Full License

Additional Declarations: No competing interests reported.

ReaxFF molecular modeling of hemp lignin transformations in supercritical CO_2–ethanol–water compared with 2D HSQC NMR observations

Yunhao Zhang[a], Yanhong Feng[a,*], Bo Lei[c], He Zhang[a], Guizhen Zhang[a], Xiaochun Yin[a], Bo Wu[b]

[a] The National Engineering Research Center of Novel Equipment for Polymer Processing, Guangdong Provincial Key Laboratory of Technique and Equipment for Macromolecular Advanced Manufacturing, School of Mechanical & Automotive Engineering, South China University of Technology, Guangzhou 510640, China

[b] National Industrial Innovation Center of Polymer Materials Co., Ltd., Guangzhou 510640, China

[c] Hubei Engineering University, Xiaogan 432000, China

* Corresponding author: Yanhong Feng (yhfeng@scut.edu.cn)

Abstract

Context: Supercritical CO_2–ethanol–water media can promote both cleavage and condensation of lignin, but the sequence of covalent reactions is difficult to resolve experimentally. Reactive molecular modeling was therefore used to examine solvent-associated transformations of hemp lignin and to compare the simulated event order with 2D HSQC NMR observations. Ether-bond cleavage preceded extensive fragmentation, followed by ethanol- and CO_2-associated reactions, phenolic-hydroxyl formation, carboxyl conversion, formaldehyde formation, and condensation at progressively higher simulated severity. Increasing treatment temperature decreased β-O-4 abundance, promoted condensed syringyl signals, and altered p-coumarate, aldehyde, and weak stilbene-like correlations. At high simulated severity, the CO_2-containing system formed more formaldehyde and retained fewer net lignin C–C bonds than the ethanol–water system. The simulation-to-experiment mapping is condition-specific and represents event ordering rather than a universal temperature conversion.

Methods: A ten-molecule hemp lignin model was constructed and equilibrated with Materials Studio and PACKMOL. Reactive molecular dynamics trajectories using a C/H/O ReaxFF parameterization were run in LAMMPS for CO_2–ethanol–water and ethanol–water boxes under continuous NVT heating from 300 to 2300 K at 2 K ps^{-1} for 1000 ps. Molecular species and reaction pathways were analyzed with MATLAB and Open Babel. Purified milled wood lignin treated at 373.15–453.15 K was analyzed by 2D HSQC NMR, and relative linkage abundances were obtained from cross-peak integrals using JEOL Delta 5.0.

Keywords: lignin; reactive molecular dynamics; ReaxFF; supercritical carbon dioxide; solvent effects; HSQC NMR

1. Introduction

Lignin is the second most abundant natural polymer after cellulose and an important renewable aromatic resource. In hemp bast (Cannabis sativa L.) fibers, lignin influences fiber processing and the value of downstream lignocellulosic products, but its structural heterogeneity makes separation-induced changes difficult to control [1, 2]. Mixed supercritical CO_2, ethanol, and water (SCEW) has shown potential for lignin fractionation. Du et al. [3] reported β-O-4 cleavage and increased hydroxyl content in corn-cob lignin, while Jiang et al. [4] described changes in lignin recovery and structure during treatment of eucalyptus. Feng et al. [5] subsequently showed that the structure of hemp lignin depends on SCEW treatment temperature. Resolving the competing cleavage, functionalization, and condensation reactions is therefore important for tuning lignin properties during hemp bast biorefining.

Reactive molecular dynamics based on the ReaxFF force field permits bond formation and cleavage during molecular dynamics and is therefore useful for exploring complex reaction networks [6, 7]. The potential energy contains the bonded, angular, torsional, conjugation, hydrogen-bonding, van der Waals, and electrostatic contributions summarized in Eq. (1) [8]:

$$E = E_{bond} + E_{lp} + E_{over} + E_{under} + E_{val} + E_{pen} + E_{coa} + E_{\mathrm{C2}} + E_{trip} + E_{tors} + E_{conj} + E_{\mathrm{H-}bond} + E_{vd\mathrm{W}aals} + E_{Coulomb} \quad (1)$$

In Eq. (1), E is the total potential energy. The remaining terms describe bond and lone-pair energies; over- and under-coordination corrections; valence-angle, penalty, and conjugation contributions; carbon–carbon and carbon–oxygen triple-bond corrections; torsional and four-body conjugation energies; and hydrogen-bond, van der Waals, and Coulomb interactions.

Chemical events that occur over experimental time scales are often inaccessible within short ReaxFF-MD trajectories. The Arrhenius relation in Eq. (2) illustrates why an elevated temperature can increase the rate at which activated events are sampled:

$$\frac{d \ln k}{dT} = \frac{E_a}{RT^2} \quad (2)$$

In Eq. (2), k is the reaction rate constant, A is the pre-exponential factor, E_a is the activation energy, R is the universal gas constant, and T is the absolute temperature. Temperature-accelerated dynamics is a formally defined rare-event method [9], whereas many reactive molecular dynamics studies use elevated temperatures or continuous heating as a practical sampling strategy [10–13]. The present work adopts the latter approach. Consequently, the observed event temperatures are trajectory-dependent descriptors used for comparison within this study; they are not direct kinetic equivalents of the experimental treatment temperatures.

ReaxFF-MD has been used to investigate lignin oxidation, pyrolysis, and gasification [14]. Examples include lignin gasification in supercritical water [15], β-O-4 dimer reactions over 1000–5000 K [16], γ-O-4 cleavage and gas formation [17], and α-O-4 dimer gasification [18]. Dimer models are useful for resolving individual pathways, but they do not capture the simultaneous evolution of functional groups and intermolecular reactions in a multi-

molecule lignin environment.

Controlled heating of larger reactive systems offers a complementary view of temperature-dependent events. Wang et al. [19] examined co-gasification of lignin and plastics in supercritical liquids, and Zhang et al. [20] investigated the influence of iron-based catalysts on lignin gasification.

Pang et al. [21] used gradual heating to study CO_2 gasification of softwood lignin from 298 to 3000 K and observed sequential ether-bond cleavage, aromatic-ring opening, and CO formation. Wang et al. [22] simulated softwood lignin gasification in supercritical CO_2. These studies show the value of reactive trajectories for ordering chemical events, but the connection between their simulation temperature windows and experimentally relevant fractionation conditions remains uncertain.

Recent work combined 2D NMR with classical molecular dynamics to examine lignin depolymerization and aggregation in sub- and supercritical water–ethanol media, identifying water–alcohol clusters and lignol aggregates [23]. Classical molecular dynamics resolves solvation and aggregation but does not describe covalent bond formation and cleavage. The present study extends this solvent-level perspective to a CO_2-containing ternary medium using ReaxFF to follow reactive trajectories and HSQC observations to compare event ordering.

The computational objective of this study was to establish the order of major solvent-mediated reaction classes in a multi-molecule lignin environment. A ten-molecule hemp lignin model, controlled-heating ReaxFF-MD simulations, and 2D HSQC NMR observations from SCEW-treated isolated lignin were combined for this purpose. Unlike the earlier study of temperature-dependent lignin extraction from intact hemp fibers [5], the present work focuses on reactive pathways in purified milled wood lignin. SCEW and ethanol–water systems were compared for ether-bond cleavage, condensation, formaldehyde formation, carboxyl conversion, and formation of stilbene- and eight-membered aryl-ether-like structures. The spectra were used to compare the order of simulated reaction classes with treatment-dependent structural changes and to construct a condition-specific empirical mapping.

2. Materials and methods

2.1. Preparation of milled wood lignin and SCEW treatment

Milled wood lignin (MWL) was prepared from hemp bast fiber (Cannabis sativa L.) for model construction and experimental comparison. Hemp bast fiber (>80 mesh, 10 g) was extracted with 300 mL of benzene–ethanol solution (2:1, v/v) in a Soxhlet apparatus for 24 h to remove extractives. The purified fiber was ball-milled with ZrO_2 balls in a planetary mill at 600 rpm for 24 h and extracted three times with 200 mL of 96% dioxane–water (96:4, v/v) at 50 °C for a total of 24 h. The combined extract was concentrated under vacuum at 50 °C and freeze-dried. The crude MWL was dissolved in 40 mL of 90% acetic acid–water (v/v), precipitated in 400 mL of deionized water, filtered, washed to neutral pH, and vacuum freeze-dried.

Purified MWL (0.5 g) was placed in a polytetrafluoroethylene liner suspended above 250 mL of an ethanol–water liquid phase with a 2:1 molar ratio. After evacuation, CO_2 was charged to an initial pressure of 6 MPa. The sealed reactor was then heated to 373.15, 393.15, 413.15, 433.15, or 453.15 K and held for 1 h. The recovered SCEW-treated lignin samples were vacuum freeze-dried and designated SCEL1, SCEL2, SCEL3, SCEL4, and SCEL5, respectively.

This isolated-MWL treatment differs from the intact-fiber extraction protocol reported previously [5]. The HSQC

spectra analyzed here correspond to the isolated-MWL sample series described above and are used to compare structural changes with the reactive trajectories.

2.2. Chemical structure analysis

Two-dimensional heteronuclear single-quantum coherence (2D HSQC) NMR spectra were acquired for the lignin samples. Approximately 50 mg of each sample was dissolved in 0.5 mL of DMSO-d_6. Spectra were recorded at a ^{1}H frequency of 500 MHz with a 5 mm probe using a standard ^{1}H–^{13}C HSQC pulse sequence. Spectral widths were 11 ppm in F2 (^{1}H) and 190 ppm in F1 (^{13}C), with 1024 and 256 data points, respectively, 64 scans, and a 1.5 s interscan delay. Contour volumes were integrated in JEOL Delta 5.0. Relative linkage abundances were calculated from the corresponding HSQC signal integrals using Eq. (3):

$$c(x) = \frac{A(x)}{0.5(S_{2,6}+S\prime_{2,6}+S_{\text{condensed}}) + G_2} \times 100\% \quad (3)$$

In Eq. (3), c(x) is the relative abundance of linkage x, and A(x) is the Cα integral for linkage x; $S_{2,6}$ and $S'_{2,6}$ are the $C_{2/6}$ integrals of syringyl and α-oxidized syringyl units, respectively; Scondensed is the $C_{2/6}$ integral assigned to condensed syringyl units; and G_2 is the C_2 integral of guaiacyl units.

3. Computational methods

3.1. Model construction

The representative lignin structure used in this study is shown in Fig. 1a. It contains the principal β-O-4, α-O-4, 5-O-4, β-5, and 5-5 linkages, together with six phenolic hydroxyl, nine aliphatic hydroxyl, seven methoxy, and one carboxyl group. The corresponding molecular model (LIG; Fig. 1b) was constructed in Materials Studio. The model was used to compare reaction trends and was not intended to reproduce the complete molecular-weight or compositional distribution of native hemp lignin.

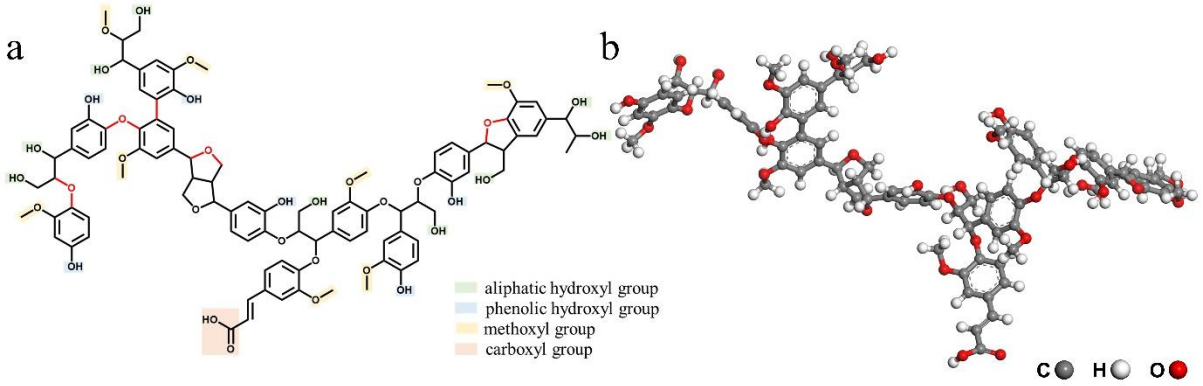


Fig. 1 Representative LIG molecule: (a) chemical structure and (b) molecular model

Ten optimized LIG molecules were packed in a periodic simulation box in Materials Studio. An initial density of 0.2 g cm^{-3} was used to limit close contacts during box construction and to provide a common starting point for the comparative trajectories. The CO_2, water, and ethanol composition was based on the CO_2-rich phase calculated with Aspen Plus at 453.15 K; the resulting molecular counts are listed in Table 1. PACKMOL was used to construct

the SCEW system (SCEL). A comparison system containing the same numbers of ethanol and water molecules but no CO_2 was constructed and is denoted EL (Fig. 2b). Because the composition was fixed, the simulations do not reproduce changes in phase density or composition across the full experimental temperature series.

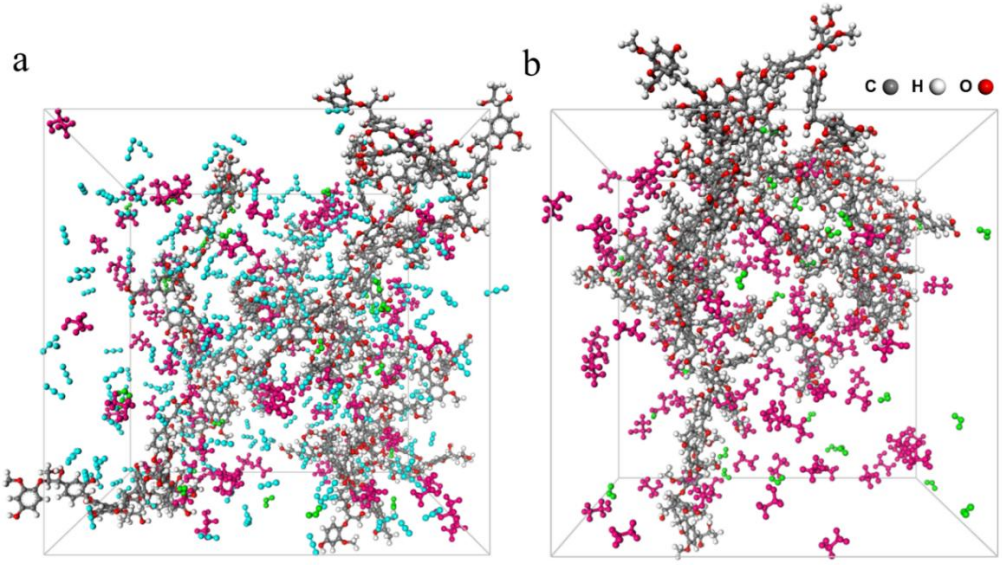


Fig. 2 Simulation boxes: (a) lignin in the SCEW system and (b) lignin in the ethanol–water comparison system. Red, green, and cyan denote ethanol, H_2O, and CO_2 molecules, respectively

Table 1 Composition of the ReaxFF-MD simulation boxes

System	Mole fractions (CO_2:H_2O:ethanol)	LIG molecules	CO_2 molecules	H_2O molecules	Ethanol molecules	Box volume (nm^3)
SCEL	0.6923:0.0743:0.2334	10	261	28	88	148.03
EL	–	10	–	28	88	148.03

3.2. ReaxFF reactive molecular dynamics simulations

All ReaxFF-MD simulations were performed with LAMMPS [24]. The packed boxes were first optimized and annealed with the Forcite module in Materials Studio. A time step of 0.25 fs was selected for stable integration of the reactive C/H/O trajectories. The simulations used a published C/H/O ReaxFF parameterization [25] that has also been applied to carbonaceous reactive systems [26]. The resulting pathways and thresholds should therefore be regarded as force-field dependent.

After energy minimization, each system was simulated in the canonical (NVT) ensemble [27]. Temperature was increased continuously from 300 to 2300 K at 2 K ps^{-1} over a total heating time of 1000 ps to sample a sequence of reactive events within the accessible trajectory time. The temperature was controlled with the Berendsen method using a damping constant of 0.1 ps [28], and the equations of motion were integrated with the Verlet algorithm. This accelerated heating protocol is used for comparative event ordering and is not a formal implementation of temperature-accelerated dynamics. Molecular connectivity was assigned using a dimensionless bond-order threshold of 0.3. Species counts were compiled in MATLAB, and representative reaction pathways

were inspected with Open Babel; the same analysis settings were applied to both systems.

Supplementary reaction schemes are provided in the Supplementary material (Figs. S1–S7).

4. Results and discussion

4.1. Carbon structure evolution of lignin during heating

Table 2 defines the carbon-number ranges used to describe products in the trajectories. As shown in Fig. 3, fragments containing 30–40 carbon atoms first accumulated as larger LIG structures fragmented and then declined as conversion progressed. Molecules in the C15–C20 and C20–C30 ranges persisted to 2300 K in both systems, consistent with the relative stability of biphenyl motifs connected through 5-5 linkages. C10–C15 species appeared near 1174 K in EL and above 1300 K in SCEL. Within these trajectories, the delayed appearance in SCEL is consistent with a different local environment around LIG in the presence of CO_2, although the simulation does not isolate a single cause for this shift.

C5–C10 products mainly contained one aromatic ring or a longer alkyl chain, whereas C3–C5 products were predominantly short-chain fragments. Aromatic-ring-containing products were more abundant than C3–C5 fragments throughout most of the heating range, and the latter accumulated mainly above 2000 K. The C5–C10 count began to rise near 1400 K in SCEL and near 1516 K in EL. These onset values describe the individual simulated trajectories and should not be interpreted as statistically resolved kinetic thresholds.

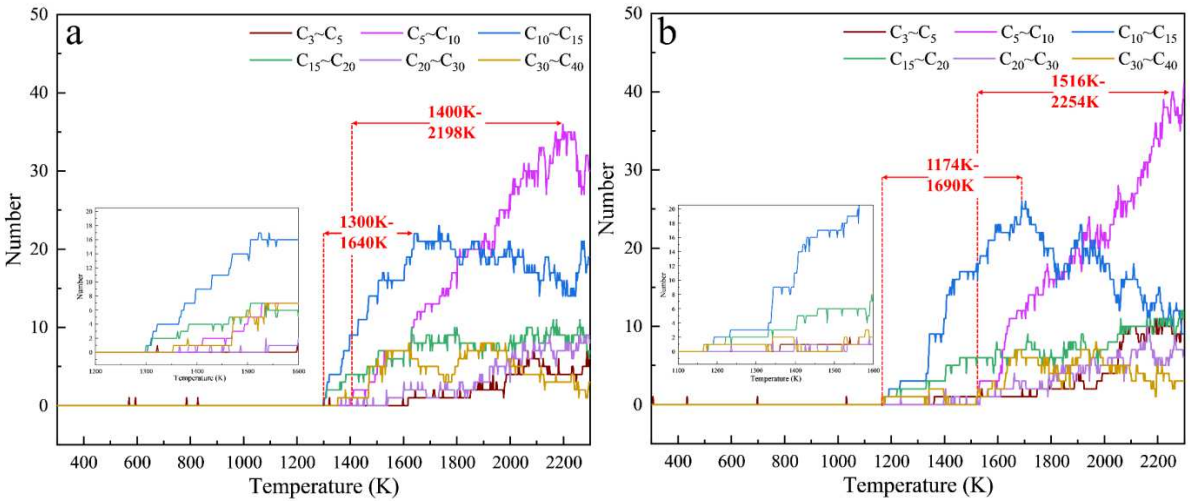


Fig. 3 Evolution of products grouped by carbon-atom count during heating: (a) SCEL and (b) EL

Table 2 Structural interpretation of product carbon-number ranges

Carbon-number range	Structural description
C3–C5	Short-chain alkyl compounds
C5–C10	One-ring aromatic or long-chain compounds
C10–C15	Lignin-derived structures with two aromatic rings
C15–C20	Lignin-derived structures with three aromatic rings

Carbon-number range	Structural description
C20–C30	Products of more extensive ether-bond cleavage
C30–C40	Products of less extensive ether-bond cleavage

4.2. Changes in CO_2 molecule count

Fig. 4 tracks the number of intact CO_2 molecules in SCEL during heating. The count began to decline near 1790 K, marking the onset of detectable CO_2 consumption in this trajectory. Representative CO_2-associated pathways observed in the trajectory are summarized in Fig. S1. They include radical addition, hydrogen transfer, and pathways that yield phenolic hydroxyl or carboxyl functionality; these structures are pathway hypotheses rather than independent evidence of a unique mechanism.

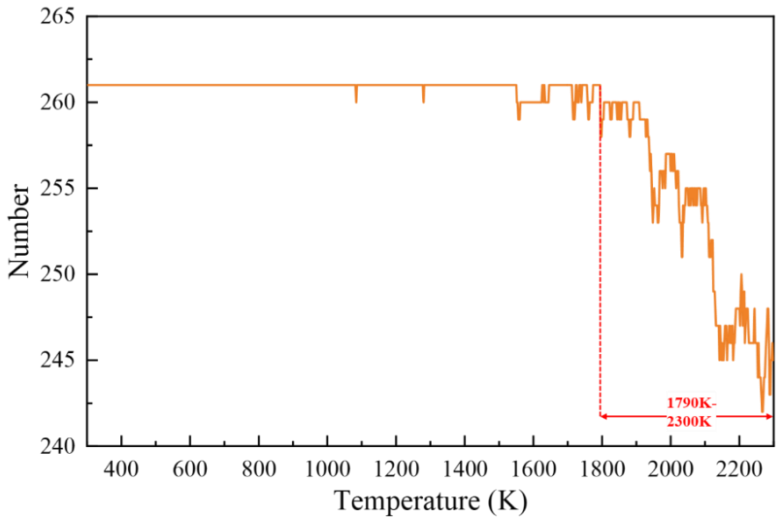


Fig. 4 Number of intact CO_2 molecules in SCEL during heating

4.3. Changes in ethanol and water quantities during heating

Figs. 5a and 5b show the numbers of intact ethanol and water molecules, respectively. Ethanol consumption began at similar temperatures in SCEL and EL, suggesting little difference in its initial reactivity between the two simulated environments. Net water formation began near 1458 K in SCEL and 1360 K in EL. Above 1900 K, the water count was lower in SCEL than in EL. Representative reactions such as R1 consume water while generating formyl-related species, and may contribute to this difference; however, the trajectory analysis does not establish a unique causal pathway.

Representative ethanol-associated events in SCEL are shown in Fig. S2 (R12–R24). Across these trajectories, ethanol frequently acted as a hydrogen donor and participated in the formation of phenolic and aliphatic hydroxyl groups. Other observed events included condensation and carbonyl-related transformations. These pathways provide a molecular interpretation of ethanol consumption but do not quantify their relative experimental contributions.

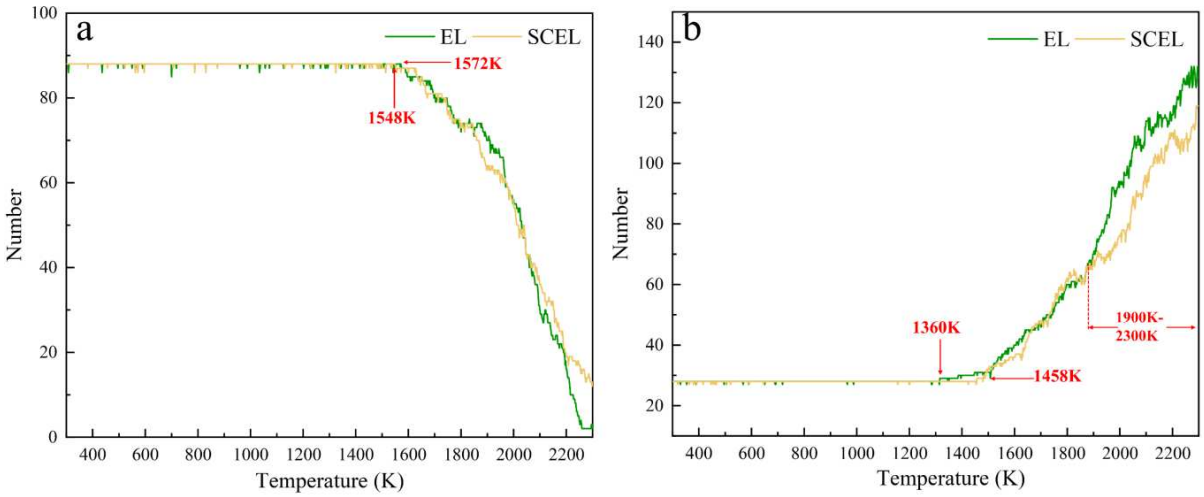


Fig. 5 Numbers of intact ethanol and H_2O molecules during heating: (a) ethanol in SCEL and EL and (b) H_2O in SCEL and EL

4.4. Formaldehyde abundance and C–C bonds during heating

Formaldehyde is a lignin-derived product that can suppress condensation under suitable conditions [29]. In both simulations, formaldehyde first appeared above approximately 1450 K and increased with temperature (Fig. 6a). Above 2040 K, its abundance was greater in SCEL than in EL. The number of lignin C–C bonds initially decreased and then rose above approximately 1660 K as condensation events accumulated (Fig. 6b). Beyond 2040 K, EL contained more C–C bonds, whereas the SCEL count approached a plateau. The opposing trends are consistent with an association between greater formaldehyde abundance and reduced net C–C bond formation in SCEL, but they do not by themselves establish formaldehyde as the sole cause.

Representative formaldehyde-forming events in SCEL are shown in Fig. S3. The observed CO_2- and radical-associated pathways offer a possible explanation for the greater formaldehyde abundance in SCEL at high simulated temperatures.

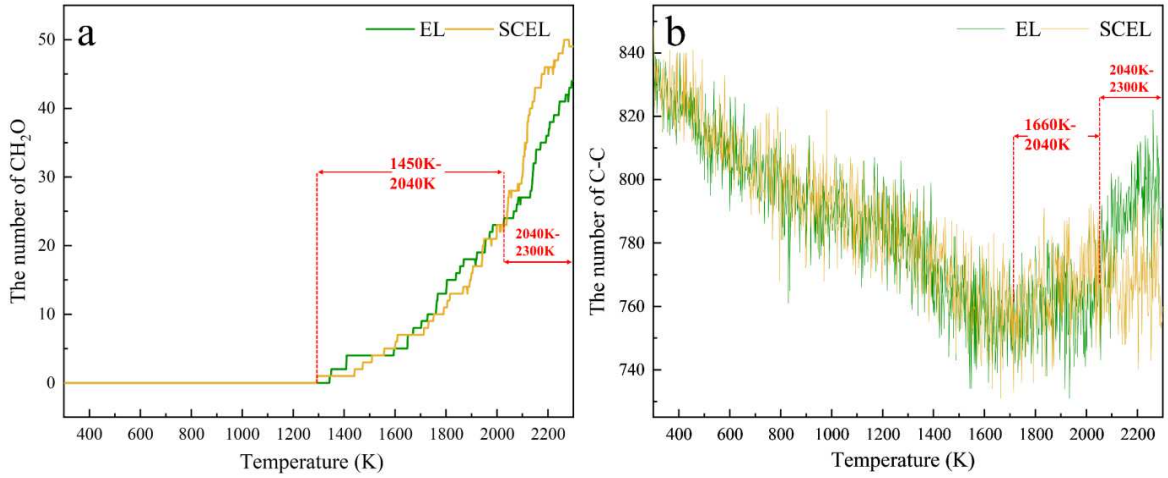


Fig. 6 Formaldehyde and lignin C–C bonds during heating: (a) number of formaldehyde molecules in SCEL and EL and (b) number of C–C bonds in LIG

4.5. Changes in ether bonds and phenolic hydroxyl groups in lignin during heating

Ether-bond cleavage is an important source of new phenolic hydroxyl groups. In Fig. 7a, the first detected

ether-bond loss occurred near 1154 K in EL and 1300 K in SCEL, consistent with the appearance of C10–C15 fragments in Fig. 3. The difference narrowed at higher temperatures as reactions became more extensive. The later onset in SCEL is consistent with altered local packing around LIG in the CO_2-containing box, but this interpretation remains qualitative.

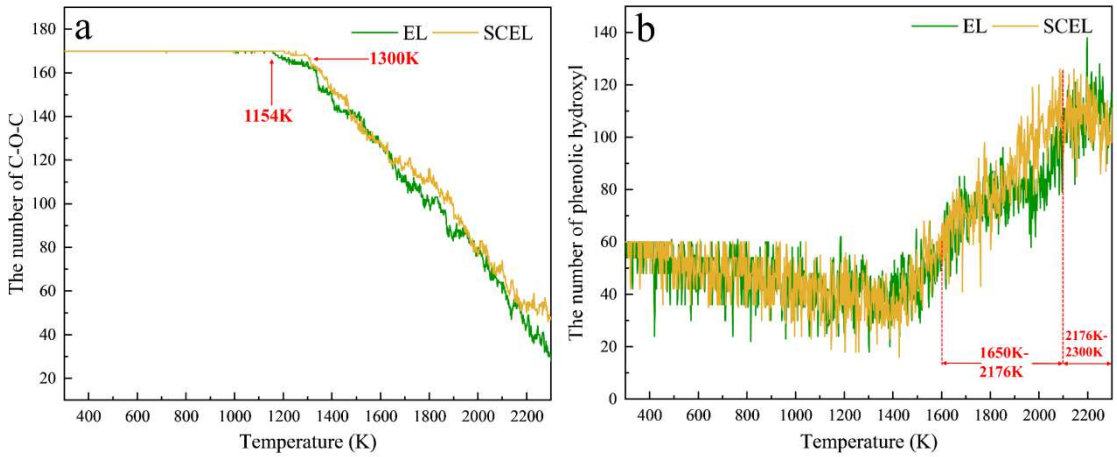


Fig. 7 Functional-group counts in LIG during heating: (a) ether bonds and (b) phenolic hydroxyl groups

The number of phenolic hydroxyl groups decreased below 1650 K, consistent with O–H homolysis and hydrogen-radical release in the simulated trajectories (Fig. 7b). Above 1650 K, ether-bond cleavage followed by hydrogen transfer generated new phenolic hydroxyl groups. The count declined again above 2176 K as additional high-temperature pathways became accessible; representative events are shown in Fig. S4.

4.6. Changes in carboxyl groups during heating

The carboxyl-group count showed an initial decrease and recovery below 1714 K in both systems (Fig. 8), reflecting reversible changes in bonding assignments during hydrogen-transfer events. Above 1714 K, the count declined to zero as carboxyl-containing structures were converted or fragmented. As elsewhere, 1714 K is a trajectory-specific onset descriptor rather than an experimental kinetic threshold.

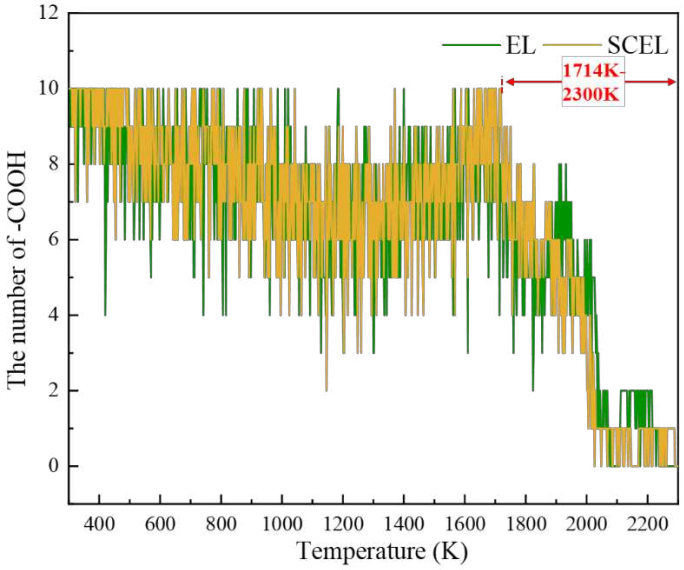


Fig. 8 Number of carboxyl groups in LIG during heating

Representative carboxyl-group pathways observed above 1714 K are summarized in Fig. S5. They include

hydrogen transfer, decarboxylation, and conversion to aldehyde-, hydroxyl-, and C–O-containing structures, which are consistent with the declining carboxyl-group count.

4.7. Formation pathways of stilbene and eight-membered aryl ether structures

Stilbene contains a 1,2-diphenylethene framework [30], and SCEW treatment has previously been proposed to favor stilbene formation in lignin [31]. In the present SCEL trajectory, stilbene-like products appeared above approximately 1980 K through several pathways (Fig. S6). Eight-membered aryl-ether-like rings appeared above approximately 2100 K through intramolecular cyclization and remained present to the end of the trajectory (Fig. S7). These pathways identify chemically plausible products within the force-field trajectory; structural assignments from the experimental spectra are considered separately below.

4.8. Comparison with 2D HSQC NMR observations

The simulated trends were compared with MWL and SCEW-treated lignin obtained at five temperatures. Fig. 9 shows the 2D HSQC spectra, Fig. 10 identifies the assigned structures, Table 3 lists the chemical shifts, and Table 4 summarizes relative structure abundances. The relative abundance of β-O-4 structure A decreased with treatment temperature, consistent with progressive cleavage of β-aryl ether linkages.

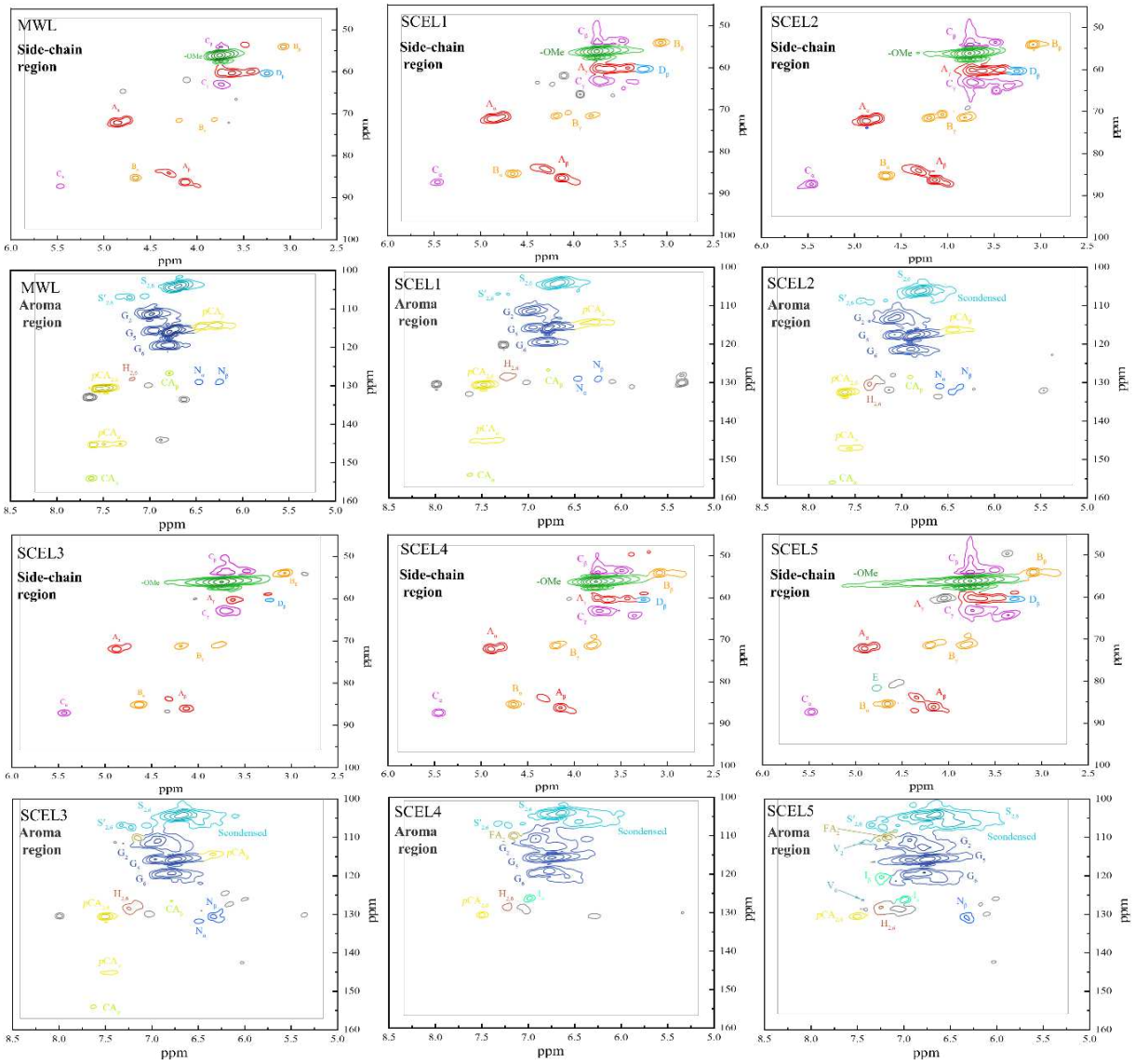


Fig. 9 2D HSQC NMR spectra of MWL and SCEW-treated lignin

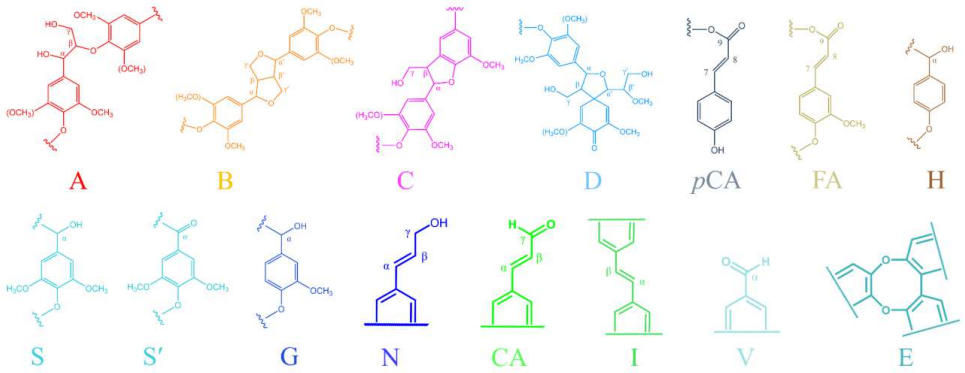


Fig. 10 Lignin structures assigned in the 2D HSQC NMR spectra

Table 3 2D HSQC NMR chemical shifts and assignments for lignin structures

δC/δH (ppm)	Chemical shift assignment
53.04/3.74	Cβ-Hβ in β-5′ phenylcoumaran substructures (Cβ)
53.93/3.06	Cβ-Hβ in β-β′ resinol substructures (Bβ)
56.17/3.74	C-H in methoxyl group (-OCH3)
59.70/3.73 and 60.34/3.41	Cγ-Hγ in β-O-4 substructures (Aγ)
62.20/4.12	Cγ-Hγ in cinnamyl alcohol end-groups (Iγ)
63.37/4.66	Cγ-Hγ in γ-acetylated β-O-4 substructures (A′γ)
69.20/4.87	Cα-Hα in β-O-4′ linked to a G-unit (Aα(G))
71.74/3.82 and 71.85/4.19	Cγ-Hγ in β-β′ resinol substructures (Bγ)
72.81/4.86	Cα-Hα in β-O-4 linked to a S-unit (Aα(S))
84.51/4.28	Cβ-Hβ in β-O-4 linked to a G-unit (Aβ(G))
85.75/4.66	Cα-Hα in β-β′ resinol substructures (Bα)
86.71/4.12	Cβ-Hβ in β-O-4 linked to a S-unit (Aβ(S))
87.70/5.45	Cα-Hα in phenylcoumaran substructures (Cα)
104.48/6.69	C2-H2 and C6-H6 in etherified S-units (S2,6)
107.10/7.20	C2-H2 and C6-H6 in α-oxidized S-units (S′2,6)
111.70/6.98	C2-H2 in G-units (G2)
115.57/6.71 and 115.84/6.95	C5-H5 in G-units (G5)
119.86/6.77	C6-H6 in G-units (G6)

Condensed syringyl signals were not detected in SCEL1, while most quantified structures decreased slightly relative to MWL and the N-structure signal increased. This pattern is compatible with limited condensation and predominantly degradative changes at 373.15 K. In the simulations, fragmentation and formation of an N-like structure (R38) occurred within the 1300–1500 K event window. The comparison supports a qualitative correspondence between these observations but does not establish a one-to-one mechanism.

Condensed syringyl signals appeared in SCEL2 at 393.15 K. Condensation events such as R41 and R45 occurred above 1600 K in the simulations, while ethanol-associated pathway R13 could contribute to N-like structures. These observations place SCEL2 in qualitative correspondence with the 1600–1700 K simulation window.

The relative p-coumarate (pCA) content decreased from 5.29% in SCEL2 to 0.26% in SCEL3. Carboxyl-related reactions R32–R34 were observed mainly between 1700 and 1800 K, providing a plausible simulation analogue for the loss of pCA-associated signals at 413.15 K.

In SCEL4, the pCA, N, and cinnamaldehyde (CA) α-position signals were no longer resolved, whereas the pCA β-position signal remained. A weak signal assigned to stilbene structure I corresponded to a relative content of 0.49%. The assignment is compatible with the stilbene-like products observed in the 1900–2000 K simulation window, although the low signal intensity warrants cautious interpretation.

SCEL5 showed signals assigned to aromatic aldehyde structure V and weak correlations associated with oxygenated carbons in structure E. Correlations from non-oxygenated carbons in an eight-membered aryl ether are expected in the crowded 120–140 ppm region and may overlap with catechol-derived signals. The experimental assignment is therefore tentative, but it is compatible with the R75-like structure observed in the 2000–2200 K simulation window.

Table 4 Semi-quantitative relative abundances of lignin structures in MWL and SCEW-treated samples

Sample	A (%)	B (%)	C (%)	Scondensed (%)	pCA (%)	CA (%)	N (%)	I (%)
MWL	45.75	10.71	5.61	–	9.88	1.74	0.74	–
SCEL1	39.65	10.35	5.42	–	7.36	0.98	1.45	–
SCEL2	35.62	9.62	5.21	15.32	5.29	0.76	2.26	–
SCEL3	33.65	8.84	4.95	20.31	0.26	0.42	1.23	–
SCEL4	29.68	6.82	3.23	26.31	–	–	–	0.49
SCEL5	23.92	5.21	2.13	36.51	–	–	–	3.71

Note: A, B, and C denote the β-O-4, β-5, and β-β linkages shown in Fig. 10; Scondensed denotes condensed syringyl units; pCA denotes p-coumarate; CA denotes cinnamaldehyde; N and I denote the structures labeled N and I in Fig. 10; – indicates not detected. Values are semi-quantitative relative HSQC integrals.

The loss of β-O-4 structures, emergence of condensed syringyl signals, decline in pCA-associated signals, and appearance of weak stilbene- and aryl-ether-like correlations follow the same broad sequence as the simulated events. This comparison provides qualitative experimental support for the ordering of reaction classes but does not independently validate the force field or the exact simulation thresholds. Table 5 therefore reports matched event windows rather than a direct temperature equivalence.

Table 5 Qualitative correspondence between experimental treatments and simulation event windows

Experimental temperature (K)	Simulation event window (K)
373.15	1300–1500
393.15	1600–1700
413.15	1700–1800
433.15	1900–2000
453.15	2000–2200

4.9. Empirical mapping of simulation and experimental temperatures

An empirical relationship was fitted to the experimentally assigned treatment points and their corresponding simulation event windows (Table 5). The resulting expression is given in Eq. (4):

$$T = C_1 + C_2 T_f + C_3 T_f^2 + \frac{C_4 k}{T_f - T_i} \quad (4)$$

In Eq. (4), T is the experimental temperature (K), Ti and Tf are the initial and final simulation temperatures (K), and k is the simulation heating rate (K ps^{-1}). The fitted constants are listed in Table 6. Because the same matched events were used to establish the parameters, the equation is a descriptive, condition-specific calibration rather than an independently validated predictive model. It should not be extrapolated to other lignins, solvent compositions, heating rates, or force-field parameterizations without additional experiments.

Table 6 Empirical parameters used in Eq. (4)

Parameter	Value
C_1	−1600.69
C_2	1.2522
C_3	−0.0002
C_4	360020.37

In this calibration, the onset of fragmentation near 1300 K corresponds to the 373.15 K treatment, ethanol-associated reactions near 1500 K map to approximately 379.52 K, and the first condensation events above 1600 K align with SCEL2. Carboxyl conversion after 1714 K and detectable CO_2 consumption near 1790 K map to approximately 404.14 and 414.66 K, respectively. Stilbene-like products in the 1900–2000 K window align with the 433.15 K treatment. Above 2040 K, greater formaldehyde abundance coincides with reduced net C–C bond formation in SCEL and maps to approximately 446.17 K. Eight-membered aryl-ether-like products in the 2000–2200 K window align with the highest-severity treatment. These mapped values are model-associated estimates, not exact kinetic thresholds.

5. Conclusions

Controlled-heating ReaxFF-MD simulations and 2D HSQC NMR observations were combined to examine how the SCEW medium influences the sequence of chemical changes in hemp lignin. The trajectories generated pathway hypotheses for ether-bond cleavage, ethanol- and CO_2-associated reactions, condensation, carboxyl conversion, and the formation of higher-severity products. The spectra provided an experimental basis for comparing the order of these reaction classes across the treatment series.

Ethanol-associated reactions preceded detectable CO_2 consumption in the simulated trajectories. At high simulated severity, the CO_2-containing medium produced more formaldehyde and retained fewer net lignin C–C bonds than the ethanol–water medium. The progressive loss of β-O-4 structures, appearance of condensed syringyl signals, decline in pCA-associated signals, and weak evidence for stilbene- and eight-membered aryl-ether-like structures followed the same broad order as the simulated events. The empirical simulation-to-experiment mapping is specific to the present force field, heating protocol, and material, so it should be used to compare event order rather than as a universal temperature conversion.

References

[1] Mondal S, Jatrana A, Maan S, Sharma P (2023) Lignin modification and valorization in medicine, cosmetics, environmental remediation and agriculture: a review. Environ Chem Lett 21:2171–2197. https://doi.org/10.1007/s10311-023-01585-3

[2] Yang T, Li Z, Wei W, Wang X, Liu F, Xu X, Liu Z (2022) Antioxidant properties of lignin extracted from cotton stalks by ethanol solution-assisted liquid hot water before and after adding supercritical CO_2. J CO_2 Util 58:101892. https://doi.org/10.1016/j.jcou.2022.101892

[3] Du B, Li W, Bai Y, Pan Z, Wang Q, Wang X, Lv G, Ding H, Zhou J (2023) Effect of CO_2 concentration on improving yield and antioxidant activity of lignin from corn cobs. Bioenerg Res 16:954–966. https://doi.org/10.1007/s12155-022-10490-6

[4] Jiang Y, Feng Y, Lei B, Zhong H (2020) Impact mechanisms of supercritical CO_2–ethanol–water on extraction behavior and chemical structure of eucalyptus lignin. Int J Biol Macromol 161:1506–1515. https://doi.org/10.1016/j.ijbiomac.2020.07.318

[5] Zhang Y, Chen H, Sun H, Liu Z, Lei B, Wu B, Feng Y (2024) Separation of lignin derivatives from hemp fiber using supercritical CO_2, ethanol, and water at different temperatures. Int J Biol Macromol 264:130390. https://doi.org/10.1016/j.ijbiomac.2024.130390

[6] Chenoweth K, van Duin ACT, Goddard WA (2008) ReaxFF reactive force field for molecular dynamics simulations of hydrocarbon oxidation. J Phys Chem A 112:1040–1053. https://doi.org/10.1021/jp709896w

[7] Senftle TP, Hong S, Islam MM, Kylasa SB, Zheng Y, Shin YK, Junkermeier C, Engel-Herbert R, Janik MJ, Aktulga HM, Verstraelen T, Grama A, van Duin ACT (2016) The ReaxFF reactive force-field: development, applications and future directions. npj Comput Mater 2:15011. https://doi.org/10.1038/npjcompumats.2015.11

[8] Liu L, Jaramillo-Botero A, Goddard WA, Sun H (2012) Development of a ReaxFF reactive force field for ettringite and study of its mechanical failure modes from reactive dynamics simulations. J Phys Chem A 116:3918–3925. https://doi.org/10.1021/jp210135j

[9] Sørensen MR, Voter AF (2000) Temperature-accelerated dynamics for simulation of infrequent events. J Chem Phys 112:9599–9606. https://doi.org/10.1063/1.481576

[10] Qiu Y, Zhong W, Yu A (2022) Simulations on pressurized oxy-coal combustion and gasification by molecular dynamics method with ReaxFF. Adv Powder Technol 33:103557. https://doi.org/10.1016/j.apt.2022.103557

[11] Salmon E, van Duin ACT, Lorant F, Marquaire PM, Goddard WA (2009) Early maturation processes in coal. Part 2: Reactive dynamics simulations using the ReaxFF reactive force field on Morwell Brown coal structures. Org Geochem 40:1195–1209. https://doi.org/10.1016/j.orggeochem.2009.09.001

[12] Zhao J, Huang Z, Jin G, Gao M, Zhu H (2021) Reaction dynamics study of hypergolic bipropellants: azide amine and dinitrogen tetroxide. Propellants Explos Pyrotech 46:1679–1686. https://doi.org/10.1002/prep.202100168

[13] Feng M, Jiang XZ, Mao Q, Luo KH, Hellier P (2019) Initiation mechanisms of enhanced pyrolysis and oxidation of JP-10 (exo-tetrahydrodicyclopentadiene) on functionalized graphene sheets: insights from ReaxFF molecular dynamics simulations. Fuel 254:115643. https://doi.org/10.1016/j.fuel.2019.115643

[14] Beste A (2014) ReaxFF study of the oxidation of softwood lignin in view of carbon fiber production. Energy Fuels 28:7007–7013. https://doi.org/10.1021/ef501901p

[15] Li H, Xu B, Jin H, Luo K, Fan J (2019) Molecular dynamics investigation on the lignin gasification in supercritical water. Fuel Process Technol 192:203–209. https://doi.org/10.1016/j.fuproc.2019.04.014

[16] Ponnuchamy V, Sandak J, Sandak A (2021) Revealing of supercritical water gasification process of lignin by reactive force field molecular dynamics simulations. Processes 9:714. https://doi.org/10.3390/pr9040714

[17] Liu X, Wang T, Chu J, He M, Li Q, Zhang Y (2020) Understanding lignin gasification in supercritical water using reactive molecular dynamics simulations. Renew Energy 161:858–866. https://doi.org/10.1016/j.renene.2020.06.022

[18] Song Z, Bai M, Yang Z, Lei H, Qian M, Zhao Y, Zou R, Wang C, Huo E (2022) Gasification of α-O-4 linkage lignin dimer in supercritical water into hydrogen and carbon monoxide: reactive molecular dynamic simulation study. Fuel 329:125387. https://doi.org/10.1016/j.fuel.2022.125387

[19] Wang T, Xu J, Liu X, He M (2022) Co-gasification of waste lignin and plastics in supercritical liquids: comparison of water and carbon dioxide. J CO_2 Util 66:102248. https://doi.org/10.1016/j.jcou.2022.102248

[20] Zhang H, Chen F, Zhang J, Han Y (2021) Supercritical water gasification of fuel gas production from waste lignin: the effect mechanism of different oxidized iron-based catalysts. Int J Hydrogen Energy 46:30288–30299. https://doi.org/10.1016/j.ijhydene.2021.06.169

[21] Pang Y, Zhu X, Li N, Wang Z (2023) Investigation on reaction mechanism for CO_2 gasification of softwood lignin by ReaxFF MD method. Energy 267:126533. https://doi.org/10.1016/j.energy.2022.126533

[22] Wang T, Liu X, Xu J, Afzal W, He M (2022) Simulation of softwood lignin gasification in supercritical carbon dioxide. J CO_2 Util 59:101959. https://doi.org/10.1016/j.jcou.2022.101959

[23] Bogdan TV, Koklin AE, Mashchenko NV, Bobrova NA, Korotaeva AM, Mishanin II, Fedoseev TV, Bogorodskiy SE, Antipova ML, Petrenko VE, Odintsova EG, Bogdan VI (2024) Experimental and simulation study of lignin depolymerization in water–ethanol sub- and supercritical medium. J Mol Liq 415:126284. https://doi.org/10.1016/j.molliq.2024.126284

[24] Thompson AP, Aktulga HM, Berger R, Bolintineanu DS, Brown WM, Crozier PS, in 't Veld PJ, Kohlmeyer A, Moore SG, Nguyen TD, Shan R, Stevens MJ, Tranchida J, Trott C, Plimpton SJ (2022) LAMMPS—a flexible simulation tool for particle-based materials modeling at the atomic, meso, and continuum scales. Comput Phys Commun 271:108171. https://doi.org/10.1016/j.cpc.2021.108171

[25] Wood MA, van Duin ACT, Strachan A (2014) Coupled thermal and electromagnetic induced decomposition in the molecular explosive α-HMX: a reactive molecular dynamics study. J Phys Chem A 118:885–895. https://doi.org/10.1021/jp406248m

[26] Hong D, Gao P, Wang C (2022) A comprehensive understanding of the synergistic effect during co-pyrolysis of polyvinyl chloride (PVC) and coal. Energy 239:122258. https://doi.org/10.1016/j.energy.2021.122258

[27] Tuckerman ME, Liu Y, Ciccotti G, Martyna GJ (2001) Non-Hamiltonian molecular dynamics: generalizing Hamiltonian phase space principles to non-Hamiltonian systems. J Chem Phys 115:1678–1702. https://doi.org/10.1063/1.1378321

[28] Berendsen HJC, Postma JPM, van Gunsteren WF, DiNola A, Haak JR (1984) Molecular dynamics with coupling to an external bath. J Chem Phys 81:3684–3690. https://doi.org/10.1063/1.448118

[29] Yang G, Gong Z, Luo X, Chen L, Shuai L (2023) Bonding wood with uncondensed lignins as adhesives. Nature 621:511–515. https://doi.org/10.1038/s41586-023-06507-5

[30] Ren X, Tian X, Cai X, Li X, Kong Q (2024) Stilbenes: a new strategy for protecting light-sensitive foods, a review of their structure classification and singlet oxygen quenching mechanism. Crit Rev Food Sci Nutr 64:9017–9031. https://doi.org/10.1080/10408398.2023.2207207

[31] Wang X, Guo Y, Zhou J, Sun G (2017) Structural changes of poplar wood lignin after supercritical pretreatment using carbon dioxide and ethanol–water as co-solvents. RSC Adv 7:8314–8322. https://doi.org/10.1039/C6RA26122A

Statements and Declarations

Funding

This work was supported by the National Natural Science Foundation of China [grant number 52273088]. The funder had no role in study design, data collection or analysis, manuscript preparation, or the decision to submit the article for publication.

Author contributions

Yunhao Zhang: Methodology, software, and writing – original draft. Yanhong Feng: Conceptualization, supervision, resources, and project administration. Bo Lei: Writing – review and editing. He Zhang: Formal analysis. Guizhen Zhang: Data curation. Xiaochun Yin: Validation. Bo Wu: Investigation. All authors read and approved the final manuscript.

Competing interests

The authors have no relevant financial or non-financial interests to disclose.

Data availability

The raw simulation inputs, processed reaction-event data, and NMR integration data supporting this study are available from the corresponding author upon reasonable request. These data have not been deposited in a public repository.

Supplementary Files

This is a list of supplementary files associated with this preprint. Click to download.

- SupplementaryInformationJMM.docx